

Article

# Sc-Modified C<sub>3</sub>N<sub>4</sub> Nanotubes for High-Capacity Hydrogen Storage: A Theoretical Prediction

Shuli Liu<sup>1</sup>, Xiao Tang<sup>2</sup>, Chang He<sup>1</sup>, Tingting Wang<sup>1</sup>, Liying Shang<sup>1</sup>, Mengyuan Wang<sup>1</sup>, Shenbo Yang<sup>3</sup>, Zhenjie Tang<sup>1</sup> and Lin Ju<sup>1,\*</sup>

<sup>1</sup> School of Physics and Electric Engineering, Anyang Normal University, Anyang 455000, China; 01958@aynu.edu.cn (S.L.); 211104005@stu.aynu.edu.cn (C.H.); 211104029@stu.aynu.edu.cn (T.W.); 211104023@stu.aynu.edu.cn (L.S.); 211104027@stu.aynu.edu.cn (M.W.); zjtang@aynu.edu.cn (Z.T.)

<sup>2</sup> College of Science, Institute of Materials Physics and Chemistry, Nanjing Forestry University, Nanjing 210037, China; xiaotang@njfu.edu.cn

<sup>3</sup> Hongzhiwei Technology (Shanghai) Co., Ltd., 1599 Xinjinqiao Road, Pudong, Shanghai 201206, China; yangshenbo@hzwtech.com

\* Correspondence: julin@aynu.edu.cn

**Abstract:** Utilizing hydrogen as a viable substitute for fossil fuels requires the exploration of hydrogen storage materials with high capacity, high quality, and effective reversibility at room temperature. In this study, the stability and capacity for hydrogen storage in the Sc-modified C<sub>3</sub>N<sub>4</sub> nanotube are thoroughly examined through the application of density functional theory (DFT). Our finding indicates that a strong coupling between the Sc-3d orbitals and N-2p orbitals stabilizes the Sc-modified C<sub>3</sub>N<sub>4</sub> nanotube at a high temperature (500 K), and the high migration barrier (5.10 eV) between adjacent Sc atoms prevents the creation of metal clusters. Particularly, it has been found that each Sc-modified C<sub>3</sub>N<sub>4</sub> nanotube is capable of adsorbing up to nine H<sub>2</sub> molecules, and the gravimetric hydrogen storage density is calculated to be 7.29 wt%. It reveals an average adsorption energy of −0.20 eV, with an estimated average desorption temperature of 258 K. This shows that a Sc-modified C<sub>3</sub>N<sub>4</sub> nanotube can store hydrogen at low temperatures and harness it at room temperature, which will reduce energy consumption and protect the system from high desorption temperatures. Moreover, charge donation and reverse transfer from the Sc-3d orbital to the H-1s orbital suggest the presence of the Kubas effect between the Sc-modified C<sub>3</sub>N<sub>4</sub> nanotube and H<sub>2</sub> molecules. We draw the conclusion that a Sc-modified C<sub>3</sub>N<sub>4</sub> nanotube exhibits exceptional potential as a stable and efficient hydrogen storage substrate.

**Keywords:** C<sub>3</sub>N<sub>4</sub> nanotube; hydrogen storage; density functional theory calculations; Sc modification



**Citation:** Liu, S.; Tang, X.; He, C.; Wang, T.; Shang, L.; Wang, M.; Yang, S.; Tang, Z.; Ju, L. Sc-Modified C<sub>3</sub>N<sub>4</sub> Nanotubes for High-Capacity Hydrogen Storage: A Theoretical Prediction. *Molecules* **2024**, *29*, 1966. <https://doi.org/10.3390/molecules29091966>

Academic Editor: Boggavarapu Kiran

Received: 4 April 2024  
Revised: 20 April 2024  
Accepted: 24 April 2024  
Published: 25 April 2024



**Copyright:** © 2024 by the authors. Licensee MDPI, Basel, Switzerland. This article is an open access article distributed under the terms and conditions of the Creative Commons Attribution (CC BY) license (<https://creativecommons.org/licenses/by/4.0/>).

## 1. Introduction

The growing developments of human communities lead to an ever-increasing demand for fossil sources of energy. This phenomenon will lead to over-exploitation and scarcity of fossil energy. Meanwhile, hazardous gases produced by burning fossil energy pollute the environment [1,2], and the released carbon dioxide also results in global warming, causing the greenhouse effect [3–6], leading to a rise in sea levels and other adverse effects [7]. Finally, the population's quality of life is significantly reduced due to damage to Earth's ecosystem. Therefore, finding an environmentally friendly alternative to solve the energy problem is urgently required [8–12]. With its plentiful reservoirs, high specific energy, good combustion characteristics, non-toxicity, non-hazardous, and non-polluting qualities, hydrogen is an extremely effective and clean energy source. Although creating hydrogen from decomposing water has advanced significantly in recent years, locating appropriate storage materials is still a major challenge [13–16]. Extensive studies on the characteristics of liquid and solid hydrogen storage materials have been initiated in an attempt to address this issue. Solid hydrogen storage materials are often a superior option, given the high

energy consumption of hydrogen liquefaction and the high requirements of hydrogen storage containers. In addition, achieving a high weight density and reversibility in terms of hydrogen storage materials is also crucial at room temperature [17–19]. Based on the US Department of Energy (US-DOE) standard [20,21], substrates are required to possess remarkable capacities for storing hydrogen while also displaying adsorption energy ranging from  $-0.2$  eV to  $-0.7$  eV for  $H_2$  molecules [22]. In addition, hydrogen storage capacity density requires being above 6.5 wt%. To identify the optimal substrate for hydrogen storage, researchers have examined various materials, including metal hydrides [23–25], metal alloys [13,26–28], metal–organic frameworks [14,29], and zeolites [30]. Yu et al. discovered that metal alloys were difficult to dehydrogenate in hydrogen storage applications and require a higher temperature for dehydrogenation [13]. Sakintuna et al. reported that magnesium-based cyanide held a reversible hydrogen storage capability of up to 7.6 wt%, but its hydrogen resolution temperature is as high as 300 degrees Celsius [25]. The difficulties encountered by these materials are high desorption temperatures and structural instability at high temperatures. Therefore, the development of materials that possess reversible hydrogen storage properties at ambient temperature is urgently needed.

Porous systems are considered viable hydrogen storage alternatives due to their good reversibility, mild hydrogen absorption/desorption conditions, and other advantages [31–33]. As a new type of porous 2D material,  $C_3N_4$  exhibits excellent hydrogen storage characteristics relating to its large porous structure, lightweight, good thermal stability, and enviable surface-to-volume ratio; therefore, it has garnered a lot of attention [34]. Previously, Chakraborty [35] et al. demonstrated the potential hydrogen storage capabilities of flat  $C_3N_4$  [36]. However, the van der Waals (vdW) interaction between  $H_2$  molecules and the pure layered nanostructures is weak, leading to low hydrogen storage capacity at room temperature. Doping or metal-modifying nanostructures are methods of improving hydrogen adsorption because the modification of metals enhances the surface activity of porous materials and further promotes their interaction with  $H_2$ . Some studies [37] have demonstrated that alkali metal doping may improve the hydrogen absorption of carbon nanotubes. Li-functionalized  $C_3N_4$  increased its hydrogen storage capacity to 10 wt%, as demonstrated by Wu et al. Notably, at 0 K, Li and  $C_3N_4$  have a low binding energy. The low binding energy would cause Li clusters to develop at a higher temperature, which would reduce the capacity of the hydrogen storage system [38]. As opposed to alkali metal elements, transition metal (TM) elements present more diverse and malleable outer electronic structures that allow them to interact with numerous substances and can alter bonding energy. Recent studies and simulations have also demonstrated that TM atoms or ions may bind hydrogen molecules and present optimal binding energies for practical uses [39–43]. Studies conducted by E. Durgun and colleagues demonstrated that a carbon atomic chain with two titanium atoms added may obtain a 14.4 wt% hydrogen storage capacity, greatly boosting the hydrogen storage mass density of carbon nanotubes [44]. Nachimuthu et al. showed that boron-doped graphene modified with TM atoms was a viable candidate material for improving reversible hydrogen storage capacity [45]. Sun et al. found that metal clusters formed by titanium atoms on carbon nanotubes altered the hydrogen binding and reduced the weight density percentage of hydrogen storage [46]. Sathe et al. found that Ti-modified  $C_{24}$  fullerene can adsorb 4  $H_2$  with 10.5 wt% hydrogen storage; however, the ultra-high desorption temperature is a severe problem [45]. Different from other TM atoms, scandium, being the lightest TM, has an abundance of vacant 3D orbitals, which are conducive to the formation of bonds with hydrogen molecules. Sc-doped  $C_{60}$  fullerene structures have shown that scandium stands out as one of the most optimal transition metal dopants for enhancing hydrogen storage in fullerene molecules. Vikram et al. also experimentally demonstrated Sc-modified carbon nanostructures as potential candidates for hydrogen storage [36]. Inspired by these reports, scandium modifications to  $C_3N_4$  nanotubes are expected to improve their hydrogen storage performance.

Our study shows that Sc-modified  $C_3N_4$  nanotubes have a strong hydrogen storage capacity and have the benefit of releasing hydrogen gas at room temperature. Based on the

simulation, Sc-modified  $C_3N_4$  nanotubes show better stability even at high temperatures, which makes it harder for the Sc atom to break free from  $C_3N_4$  nanotubes. Moreover, a strong migration barrier keeps Sc atoms stable inside the macrocycle and inhibits the creation of metal clusters. First-principles density-functional theory simulations demonstrate that  $H_2$  has a higher probability of diffusing along the tube; Sc-modified  $C_3N_4$  nanotubes have the capacity to adsorb up to nine hydrogen molecules; their hydrogen storage mass density can reach 7.287 wt%; and the average binding energy is  $-0.20$  eV/ $H_2$ , which is compliant with US Department of Energy regulations. Charge density and Bader charge analyses were performed to investigate the adsorption mechanism of Sc-modified  $C_3N_4$  nanotubes in terms of absorbing  $H_2$  molecules. The results show that there is a weak van der Waals connection and Kubas interaction between Sc atoms and  $H_2$  gas. Sc-modified  $C_3N_4$  nanotubes had an average desorption temperature of 258 K, indicating that the structure may desorb the  $H_2$  at  $-15$  °C without the need for further energy. As a result, Sc-modified  $C_3N_4$  nanotubes perform very well as a hydrogen storage medium. Our findings may provide a path to developing a novel, highly effective hydrogen storage material that can utilize hydrogen at normal temperatures and store it at low temperatures.

## 2. Results and Discussion

### 2.1. Geometric Structures of Pure $C_3N_4$ Nanotube and Single $H_2$ Molecule Adsorption

We first investigated the geometric structures of  $C_3N_4$  nanotubes and  $H_2$  molecule adsorption properties. As shown in Figure S1,  $C_3N_4$  nanotubes possess rich pore structures with a large specific surface area, which is favorable for exposing more active sites, effectively improving hydrogen storage capacity. Based on its structural characteristics, it can be found that there exist eight potential locations for the adsorption of hydrogen on pure  $C_3N_4$  nanotubes. This includes k1 and k3 (above the C atom in the pore), k2 and k4 (above the N atom in the pore), k5 and k6 (above the hexagonal ring), and k7 and k8 (above the two adjacent and next-to-next adjacent N atoms in the macrocycle). Therefore, we studied the adsorption of  $H_2$  at different sites of  $H_2$  at different sites of pure  $C_3N_4$  nanotubes. According to Formula (1), the adsorption energy of a  $H_2$  molecule on pure  $C_3N_4$  is calculated to measure the change in energy during adsorption. The adsorption energy of hydrogen at different adsorption sites is shown in Figure S2. Due to the lowest adsorption energy, k8 is the most possible adsorption site for  $H_2$  molecules, and the corresponding relaxed configuration for the adsorption system is shown in Figure 1. The  $H_2$  molecule is about 3 Å away from the surface of the nanotube, indicating weak physisorption. Moreover, the adsorption energy of all sites considered for the pure  $C_3N_4$  nanotube does not satisfy the range (DOE-US) of  $-0.2$  eV $\sim$  $-0.7$  eV. In other words, pure  $C_3N_4$  nanotubes are not suitable for hydrogen storage materials because the adsorption energy of  $H_2$  on pure  $C_3N_4$  nanotubes is too unstable.

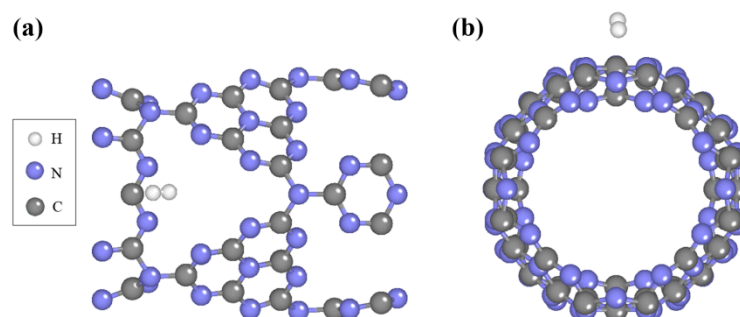


**Figure 1.** The figure shows the (a) top and (b) side views of the most stable adsorption systems of  $H_2$  on the surface of a pure  $C_3N_4$  nanotube.

### 2.2. Structure and Stability of Sc-Modified $C_3N_4$ Nanotubes

Modifications to  $C_3N_4$  materials using Sc metal are expected to improve the stability of  $H_2$  molecule adsorption. The locations at which Sc atoms are incorporated can influence the

structural stability and the efficacy of hydrogen storage in  $C_3N_4$  nanotubes. Considering the potential locations of  $H_2$  adsorption in Figure S1, we studied modifying k1–k8 of pure  $C_3N_4$  using Sc atoms to obtain a stable structure. After structural optimization, their bonding energies were calculated with Formula (2), and the results are listed in Table S1. A negative bonding energy between isolated Sc atoms and pure  $C_3N_4$  nanotubes indicates an exothermic reaction, which suggests structural stability. The optimized structures of Sc-modified  $C_3N_4$  nanotubes at the k7 and k8 sites tend to end up in the same configuration, and we found that both of the sites present the smallest bonding energy when comparing all of the obtained bonding energies of Sc atoms at different desorption sites in  $C_3N_4$  nanotubes. Therefore, the macrocycle's core is the most stable location for metal Sc atoms to adsorb in nanotubes. As shown in Figure 2, every macrocycle favoring a single Sc atom when Sc atoms are modified on  $C_3N_4$  could avoid the clustering issue for Sc decoration in  $C_3N_4$  nanotubes. An analysis of the elastic modulus reveals that single-atom Sc decoration has a minimal impact on the mechanical properties (a bit softer) of the  $C_3N_4$  nanotubes. For further details, refer to the Supplementary Materials and Figure S3.

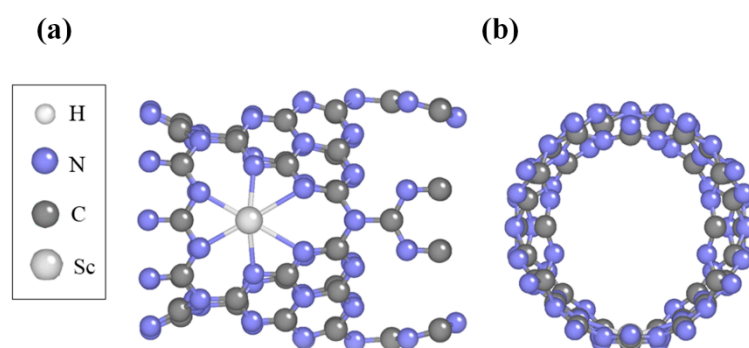


**Figure 2.** The figure shows the (a) top and (b) side views of the optimal configuration of a Sc-modified  $C_3N_4$  nanotube.

The interplay between Sc atoms and  $C_3N_4$  nanotubes was examined using the total density of states (DOS). Figure 3a demonstrates that the DOS of pure  $C_3N_4$  nanotubes exhibit symmetry between the up and down spins due to their nonmagnetic behavior ( $\mu = 0 \mu_B$ ). However, in Figure 3b, the introduction of Sc atoms into  $C_3N_4$  nanotubes breaks the symmetry of the up and down spins, resulting in spin polarization and the emergence of a magnetic moment in the Sc-modified  $C_3N_4$ . The band gap of the pure  $C_3N_4$  nanotube is calculated to be 1.40 eV, whereas the Sc-modified  $C_3N_4$  nanotube lacks a band gap and exhibits a metal-like nature. It is evident that the doping of Sc atoms in the  $C_3N_4$  nanotubes alters the electronic structure of the substrate, which makes the nanotubes more metallic. It is anticipated that this might increase the hydrogen storage capacity of Sc-modified  $C_3N_4$  nanotubes as they have more active electrons interacting with  $H_2$  molecules. To uncover the nature of orbital interactions and understand the binding process within Sc-modified  $C_3N_4$  nanotubes, we have analyzed the differences in the partial density of states (PDOS) and charge density. As shown in Figure 3c, Sc doping results in numerous new hybridization peaks at the Fermi energy level for the Sc-3d and N-2p orbitals. The hybridization between N and Sc atoms elucidates a strong orbital interaction between Sc atoms and  $C_3N_4$  nanotubes. Additionally, an increase in the DOS can lead to the formation of chemical bonds, which forecasts the superior bonding energy and enhanced structural stability of Sc-modified  $C_3N_4$  nanotubes. To further determine the precise number of electrons transferred from the Sc atoms, we conducted Bader charge analysis. The analysis revealed that each Sc atom transferred 1.83 e to the N-2p orbital of the  $C_3N_4$  nanotubes. Then, as shown in Figure 3d, we plotted three-dimensional (3D) charge density difference (CDD) images. Figure 3c,d support the notion that in the bonding mechanism between Sc and  $C_3N_4$  nanotubes, some electrons migrate from the 3D orbitals of single Sc atoms to the 2p orbitals of N atoms, thus forming covalent bonds. Based on the above analysis, it can be

inferred that the combined interactions between Sc atoms and  $C_3N_4$  nanotubes, with Sc atoms transferring 1.83 e to N atoms, form covalent bonds that can stabilize the system.

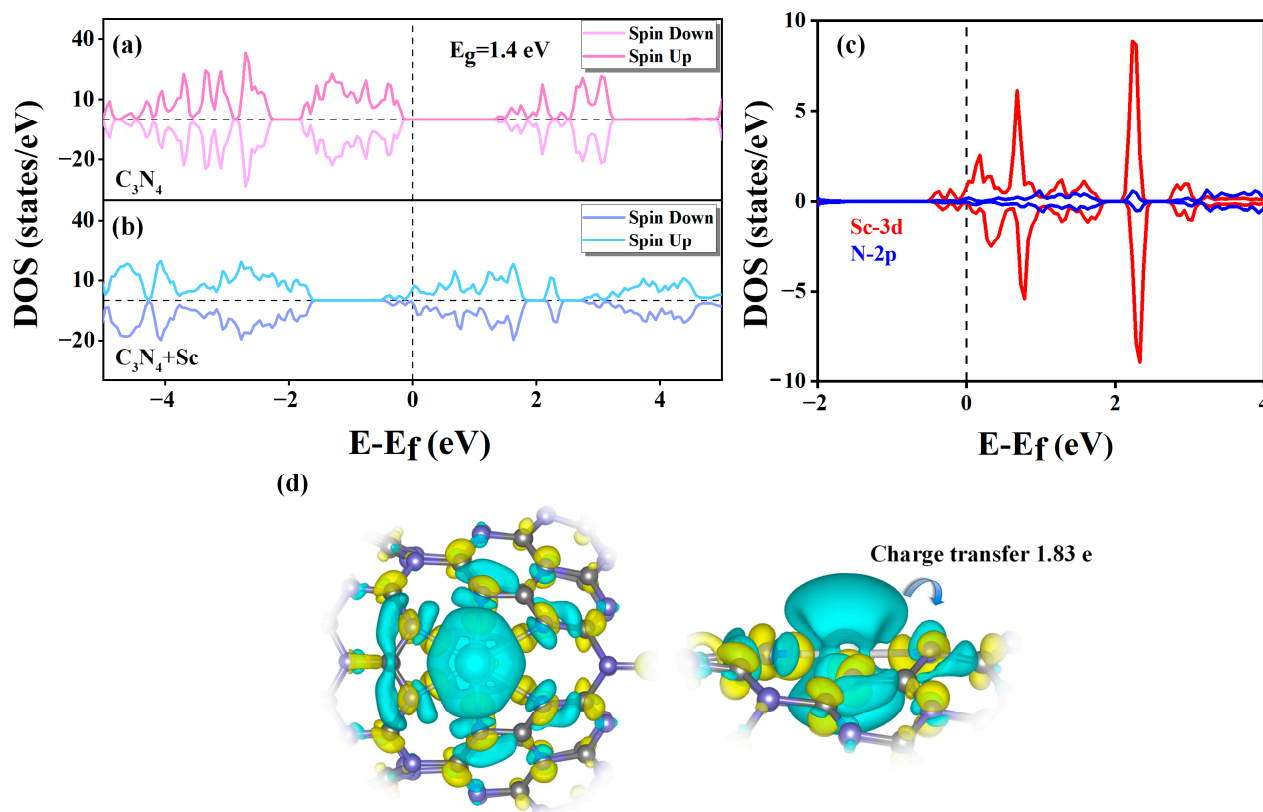


**Figure 3.** The figure shows the DOS of (a) pure  $C_3N_4$  nanotube and (b) Sc-modified  $C_3N_4$  nanotube. (c) PDOS for Sc-3d orbitals and N-2p orbitals in Sc-modified  $C_3N_4$  nanotubes. Fermi level is set at 0 eV. (d) The CDD of Sc-modified  $C_3N_4$  system with the isosurface value of  $0.003$  e/ $\text{\AA}^3$ . Cyan and yellow regions separately represent the electron-rich and electron-deficient regions.

The stability of a hydrogen storage system influences hydrogen storage performance; therefore, we performed diffusion energy barrier calculation to determine the stability of Sc atoms in each macrocycle, and ab initio molecule dynamics (AIMDs) simulations relating to a Sc-modified  $C_3N_4$  nanotube were applied to measure the structural integrity at high desorption temperatures. The clustering of metal atoms within the system can occur readily if the transition metal atom's diffusion energy barrier is close to its thermal energy at the highest desorption temperature. Therefore, we first calculated Sc-atom thermal energy at the peak resolved temperature of 500 K according to the following equation:  $E = 3/2k_B T$ , where  $k_B$  and  $E$  represent the Boltzmann constant and the thermal energy of the Sc atom, respectively. Furthermore, the value of  $T$  was set at 500 K, which exceeds the desorption temperature. The calculated thermal energy is about 0.065 eV. Then, we moved the Sc atoms from one equilibrium position to the next neighboring equilibrium position, as shown in Figure 4a. The corresponding migration barriers of Sc atoms were calculated, and the obtained values are plotted in Figure 4b. The obtained maximum migration barrier is 5.10 eV, which greatly exceeds the aforementioned thermal energy (0.065 eV), suggesting that it takes a large amount of energy for Sc atoms to jump from the center of one macrocycle to another. The results of migration barriers calculated with other exchange-correlation functional also support this opinion. More details can be found in the Supplementary Materials. Hence, the Sc-modified  $C_3N_4$  nanotubes possess high stability, i.e., the Sc atoms are not susceptible to metal agglomeration. Given that the substrate's structural integrity during heat variations is related to the durability of the hydrogen storage substrate at high desorption temperatures. Therefore, for the real-world utilization of Sc-modified

$C_3N_4$  nanotubes as hydrogen storage materials, ensuring their structural stability under high desorption temperatures is very essential. Next, we performed AIMD simulations to examine the stability of the Sc-modified  $C_3N_4$  nanotube at 500 K. As displayed in Figure 4c, the total energy of the Sc-modified  $C_3N_4$  system oscillates around the mean value of the 500 K simulation time data with small variations, which indicates that the system is structurally robust at high temperatures. In addition, many metal-doped g- $C_3N_4$  catalysts have been fabricated experimentally [47–49]. Therefore, Sc-modified  $C_3N_4$  nanotubes are feasible.

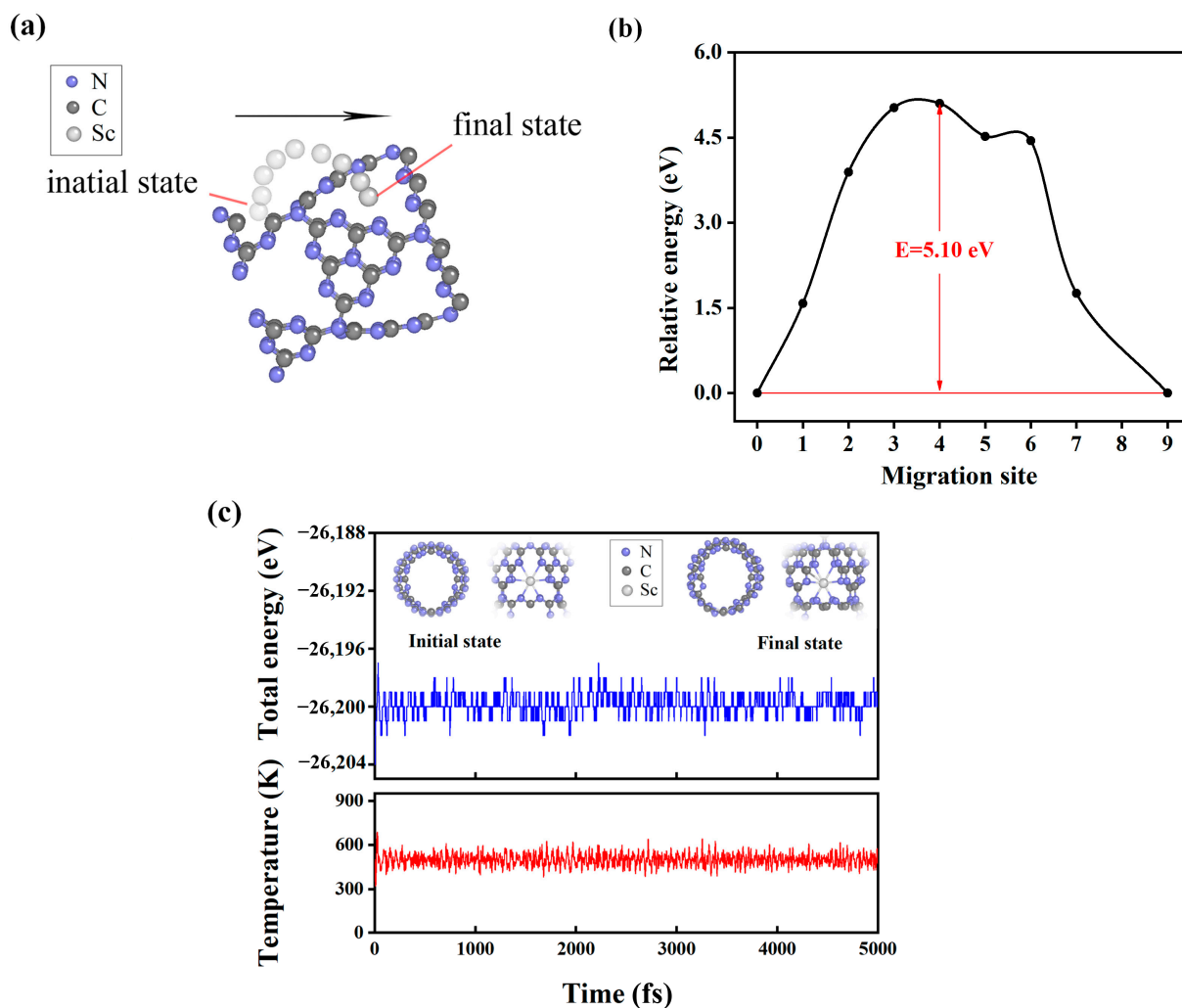


**Figure 4.** The figure shows (a) schematic diagram of migration path of Sc atoms from one equilibrium position to the next neighboring equilibrium position. (b) The corresponding diffusion energy barrier. (c) AIMD simulation on the change of the total energy Sc-modified  $C_3N_4$  nanotubes for 5 ps with a time step of 1 fs at 500 K. The corresponding temperature over all simulation time.

### 2.3. $H_2$ Molecules Adsorption on Sc-Modified $C_3N_4$ Nanotubes

In Sc-modified  $C_3N_4$  nanotubes, we discovered that hydrogen was adsorbed at the position of Sc single atom, and we calculated the average absorption energy of hydrogen molecules. First, the initial hydrogen molecule was positioned 2.487 Å away from the Sc-modified  $C_3N_4$  nanotubes. After optimizing this structure, the hydrogen molecule was changed to 2.255 Å, and the calculated adsorption energy was  $-0.79$  eV. We can conclude that the adsorption energy of the first  $H_2$  molecule is larger than the adsorption energies of  $H_2$  molecules guided by DOE-US ( $-0.2$  eV to  $-0.7$  eV). This suggests that the first hydrogen molecule has a stronger ability to be absorbed on Sc-modified  $C_3N_4$  nanotubes. Additionally, by considering structural symmetry, we examined the potential

adsorption locations for each extra hydrogen molecule. To comprehensively explore the adsorption capacity of Sc-modified  $C_3N_4$  nanotubes, we added hydrogen molecules in turn (Figure S4) and calculated the changes in H-H bond length and average adsorption energy. The computational results are shown in Figure 5a. Obviously, as the count of  $H_2$  molecules rises, the average adsorption energy tends to diminish. When nine  $H_2$  molecules are added, the average adsorption energy reaches the upper limit of the DOE-US standard ( $-0.2$  eV) [21]. This indicates that with the ongoing addition of  $H_2$  molecules,  $H_2$  molecules will inhibit interactions with the substrate and might escape into free  $H_2$  molecules. Hence, we determined that nine molecules may represent a likely limit for full hydrogen saturation per Sc atom. The optimized maximum adsorption configuration is shown in Figure 5b, where nine hydrogen molecules can be adsorbed near each Sc atom. As shown in Figure S5, we combined a Sc atom at the most stable position of each large ring and obtained a mass fraction of 19.7 wt% of Sc elements, according to Formula (3). Based on Formula (4), the final hydrogen storage mass density of the Sc-modified  $C_3N_4$  nanotubes reached 7.29 wt%, exceeding the DOE-US standard (6.5 wt%) [21], and is superior to many other hydrogen storage systems, such as Ti-decorated boron-doped twin-graphene (4.95 wt%) [50] and Sc-decorated graphene with pyridinic-N defects (4.95 wt%) [51]. The corresponding H-H bond length increases from  $0.75 \text{ \AA}$  to  $0.77 \text{ \AA}$ , which is close to the isolated hydrogen bond length, confirming that  $H_2$  molecular stability forms after adsorbing on the nanotube. In addition, we considered the effect of defects (C and N point defects) and humid environments on hydrogen storage efficiency and stability. The calculated results demonstrate that, though the introduction of defects could enhance the stability of Sc atom decoration in  $C_3N_4$  nanotubes, it brings about poor adsorption energy for the  $H_2$  molecule, reducing hydrogen storage efficiency and stability. The adsorption energy of  $H_2$  molecules increases to  $0.073$  eV in a humid environment. Such high adsorption energy means that this system cannot adsorb  $H_2$  in this case. The possible reason for this is that  $H_2O$  molecules are passive in the active site of  $H_2$  adsorption and hinder the adsorption of  $H_2$  molecules (Figure S6). The details can be found in the Supplementary Materials.

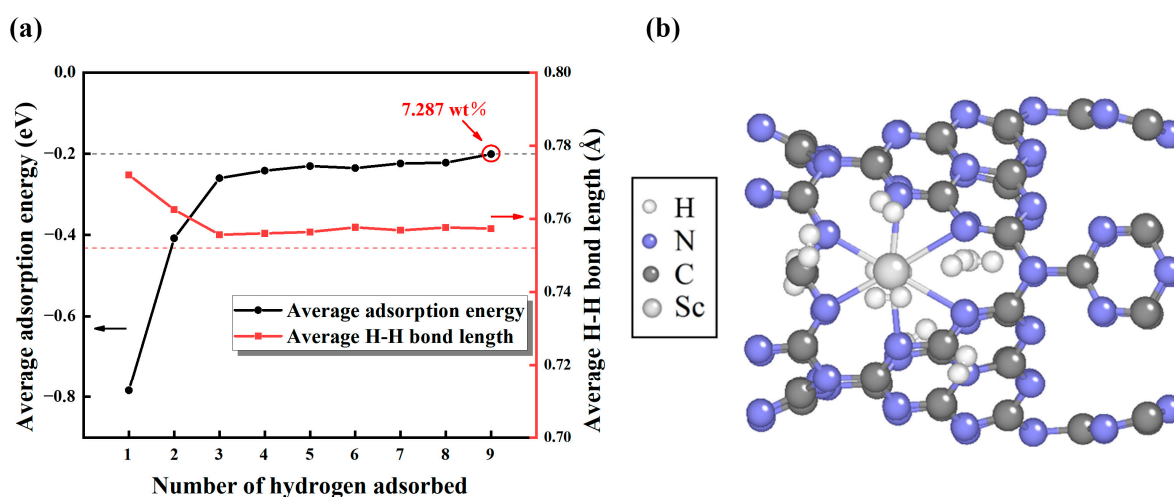


**Figure 5.** The figure shows (a) average H-H bond length and adsorption energy of 1–9 hydrogen adsorbed on Sc-modified  $C_3N_4$  nanotubes. The black dotted line shows  $E_{\text{ads}} = -0.2$  eV, and the red dotted line shows the isolated hydrogen bond length  $l = 0.752 \text{ \AA}$ . (b) The configuration of Sc-modified  $C_3N_4$  nanotubes with nine  $H_2$  molecules adsorbed.

#### 2.4. Interaction between $H_2$ and Sc-Modified $C_3N_4$ Nanotube

Figure 6 illustrates our analysis of the PDOS for H-1s and Sc-3d orbitals, which aided in understanding the mechanics of charge transfer and the interaction between the electronic orbitals of Sc-modified  $C_3N_4$  nanotube and the adsorbed  $H_2$  molecules. In Figure 6a,b, compared with isolated hydrogen molecules, H-1s orbital eigenstates are strengthened after  $H_2$  is adsorbed on Sc-modified  $C_3N_4$  tubes, which suggests that the H-1s orbital gains

charge. In addition, in Figure 6c,d, the Sc-3d orbitals eigenstates are weakened and lose charge. Hence, the improved hydrogen storage capacity of Sc-modified  $C_3N_4$  nanotubes can be attributed to the charge migration from the Sc-3d orbitals to the H-1s orbitals upon the absorption of  $H_2$  by the Sc-modified  $C_3N_4$  nanotube. As discussed above, the H-H bond length elongates slightly after the hydrogen molecule is absorbed on the Sc-modified  $C_3N_4$  nanotubes. It can be speculated that this charge transfer leads to the slight elongation of the H-H bond. To confirm this conjecture, we also calculated the differential charge and plotted the charge density of three-dimensional images to analyze the charge transfer situation, as shown in Figure 6e. Observing the charge density images, we can observe that both  $H_2$  and Sc atoms have both charge loss regions and charge gain regions, indicating that there is both charge donation and back donation in the two atoms. When hydrogen molecules are adsorbed onto the scandium-modified  $C_3N_4$  nanotube, a reverse charge transfer occurs from the scandium's filled 3D orbitals to the hydrogen's vacant lowest unoccupied molecular orbitals. Simultaneously, there is also a charge transfer from the hydrogen's filled highest occupied molecular orbitals to the unoccupied 3D orbitals of scandium. The H-1s orbital gains a little net charge (0.02 e) during the processes of charge donation and back donation, which can promote orbital interactions and lengthen the H-H bond. Therefore, the Kubas interaction and weak van der Waals interactions are primarily responsible for the binding of hydrogen molecules with the scandium atom [35]. To further explain the Kubas interaction, we plotted the PDOS of the H-1s orbital from the hydrogen adsorbed versus the Sc-3d orbital from the substrate in Figure S7. At the near-Fermi energy level, the hybrid peak of the H-1s orbital and Sc-3d orbital is almost in the same energy range, which indicates that the H-1s orbitals appear to be coupled to the Sc-3d orbitals.

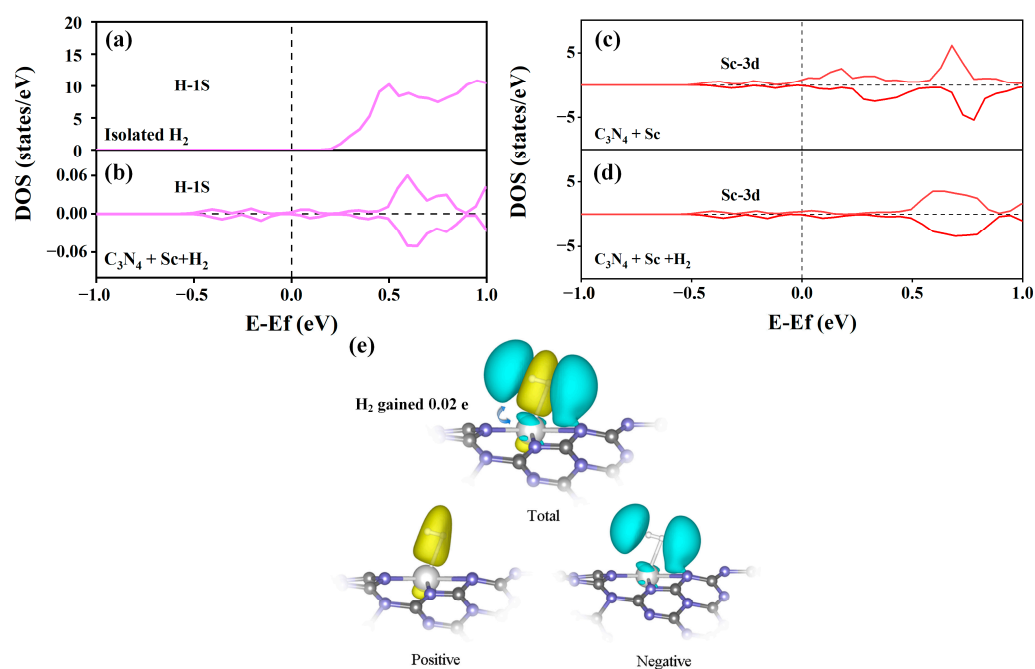


**Figure 6.** The figure shows the PDOS of the H-1s orbitals of (a) the isolated  $H_2$  molecule and (b)  $C_3N_4 + Sc + H_2$  system. PDOS of Sc-3d orbital of (c)  $C_3N_4 + Sc$  and (d)  $C_3N_4 + Sc + H_2$  systems. (e) The CDD of  $C_3N_4 + Sc + H_2$  system with the isosurface value of  $0.003 e/\text{\AA}^3$ . Cyan and yellow regions represent the electron-rich and electron-deficient areas, respectively.

### 2.5. Diffusion Energy Barrier for Hydrogen in a Tube

The distribution of adsorbed  $H_2$  on both sides of the nanotubes provides the basis for the hydrogen desorption capacity that was previously described. Therefore, we must figure out the probability of hydrogen getting inside the nanotube. Obviously, there are two ways that  $H_2$  can enter the interior: either entering the interior through the macrocycle in the side wall or via diffusion along the tube channel. To confirm the feasibility of the two pathways,

we computed the relevant diffusion energy barriers, respectively. Initially, we looked into the first case. Figure 7a depicts the detailed path of  $H_2$  diffusing along the macrocycle into the interior. The computed diffusion barriers are plotted in Figure 7b. It can be found that an energy of  $-9.91$  eV is required for  $H_2$  to enter the tube's interior through the macrocycle, which is too high to handle. In the second scenario, as displayed in Figure 7c, we conducted  $1 \times 1 \times 2$  cellular expansions of the  $C_3N_4$  nanotube to diffuse  $H_2$  molecules from one Sc adsorption site to the neighboring Sc site and, subsequently, through the  $C_3N_4$  tube channel along the z-axis. Figure 7d presents a plot of the estimated diffusion barriers. According to the findings, the  $H_2$  diffusion barriers are close to 0 eV, indicating that the  $H_2$  diffusion barrier is low along the tube channel of the  $C_3N_4$  nanotube. As a result, we propose that  $H_2$  diffuses more readily along the channel than along the macrocycle in  $C_3N_4$  nanotubes. Favorable conditions for  $H_2$  molecule transfer on Sc-modified  $C_3N_4$  nanotubes are provided by a low diffusion barrier, which ensures efficient  $H_2$  molecule adsorption and desorption capacity.

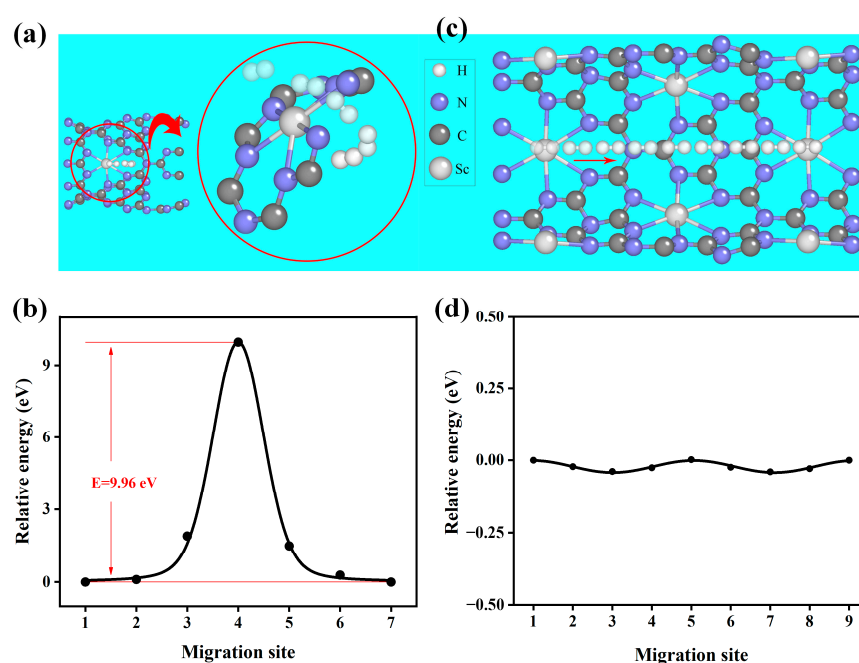


**Figure 7.** The figure shows the (a) schematic diagram of  $H_2$  diffusion in the macrocycle of  $C_3N_4$  nanotubes. The arrow means the direction of the  $H_2$  migration. (b) The energy barrier for  $H_2$  diffusion in the macrocycle of  $C_3N_4$  nanotubes. (c) Schematic diagram of  $H_2$  diffusion along the inner channel of  $C_3N_4$  nanotubes. The arrow shows the direction of  $H_2$  diffusion. (d) The energy barrier of  $H_2$  diffusion along the channel of  $C_3N_4$  nanotubes.

## 2.6. Molecule Dynamics for $H_2$ Desorption

Based on the Van Hove equation (Formula (5)), the obtained average desorption temperature is 258 K, lower than room temperature, which indicates that Sc-modified  $C_3N_4$  nanotubes can release adsorbed hydrogen at near-ambient temperatures. The release temperatures for certain hydrogen storage substances are notably greater compared to ambient conditions [7,17]. This leads to a slow release rate in terms of adsorbed hydrogen at room temperature and cannot be used normally. Therefore, high-temperature treatments are applied to achieve the rapid desorption of hydrogen; however, high temperatures will destroy the structure of hydrogen storage materials. In contrast, Sc-modified  $C_3N_4$  nanotubes can store hydrogen at low temperatures and release it at ambient temperatures for use, as shown in Figure S8. This will reduce energy consumption when facilitating the release of hydrogen, reaching about 10 kJ/mol  $H_2$  molecules compared with the case of some hydrogen storage materials containing  $MgH_2$  under standard conditions (referring to the section named “Energy Saving Compared with Some Hydrogen Storage Materials” in

the Supplementary Materials). The low desorption temperature also protects the structural stability of the hydrogen storage system and increases its service life. Consequently, Sc-modified  $C_3N_4$  nanotubes, boasting optimal average adsorption energy and release temperatures, have emerged as excellent candidates for fuel cell technologies.

### 3. Computation Details

The Device Studio software package (Version V2023A) [52] was employed to construct the computational models. DS-PAW software (Version V2023A) [53] was used to realize the simulation calculation of DFT, where Perdew–Burke–Ernzerhof (PBE) and generalized gradient approximation (GGA) [54] are adopted. The DFT has proven to be a reasonable calculation method and has been widely used to predict and verify hydrogen storage performance [55–58]. The DFT-D3 in the Grimme scheme was used to describe the van der Waals correction to simulate the various properties of  $C_3N_4$  [59]. To reduce the interaction between  $C_3N_4$  nanotubes, we placed  $C_3N_4$  nanotubes in a  $19 \text{ \AA} \times 19 \text{ \AA} \times 12 \text{ \AA}$  box for simulation. Since the vacuum spaces were all greater than  $10 \text{ \AA}$  in the x-y plane, we can consider that there is almost no interaction between the mirror samples. In the process of structural optimization, to ensure the accuracy of the simulation, we set the cutoff energy to 450 eV, and set the convergence limits of force and energy to  $0.05 \text{ eV/\AA}$  and  $10^{-4} \text{ eV}$ , respectively. To study the thermal stability of Sc-modified  $C_3N_4$  nanotubes, we conducted AIMD simulations, where this system was maintained for 5ps at a temperature setting of 500 K.

The adsorption energy for a single  $H_2$  molecule  $E_{b-H_2}$  on pure  $C_3N_4$  nanotubes, indicating the change in energy during adsorption, is established as follows [60,61]:

$$E_{b-H_2} = E_{total} - E_{H_2} - E_{sub} \quad (1)$$

where  $E_{total}$ ,  $E_{H_2}$ , and  $E_{sub}$  are the total energy of the adsorption system, isolated  $H_2$  molecule, and pure substrate ( $C_3N_4$  or Sc-modified  $C_3N_4$  nanotubes used in our study), respectively.

The bonding energies of a single Sc atom on pristine  $C_3N_4$  can be obtained with the following formula:

$$E_{b-Sc} = E_{Sc+C_3N_4} - E_{Sc} - E_{C_3N_4} \quad (2)$$

where  $E_{Sc+C_3N_4}$ ,  $E_{Sc}$ , and  $E_{C_3N_4}$  are the total energy of Sc-modified  $C_3N_4$  nanotubes, isolated Sc atoms, and pure  $C_3N_4$  nanotubes, respectively.

The mass fraction of Sc atom on  $C_3N_4$  nanotubes can be obtained with the following formula:

$$Sc - wt\% = \frac{m_{Sc}}{m_{Sc+C_3N_4}} \times 100\% \quad (3)$$

$Sc - wt\%$ ,  $m_{Sc}$ , and  $m_{Sc+C_3N_4}$  denote the mass fraction of the Sc atom, the mass of Sc atoms, and the mass of the system of Sc +  $C_3N_4$  nanotubes.

The mass fraction of  $H_2$  on Sc-modified  $C_3N_4$  nanotubes can be obtained with the following formula:

$$H_2 - wt\% = \frac{m_{H_2}}{m_{Sc+H_2+C_3N_4}} \times 100\% \quad (4)$$

$H_2 - wt\%$ ,  $m_{H_2}$ , and  $m_{Sc+H_2+C_3N_4}$  denote the mass fraction of the hydrogen, the mass of  $H_2$ , and the mass of the system of  $H_2$  and Sc-modified  $C_3N_4$ , respectively.

To test the thermal stability and reversibility of the  $H_2@Sc$ -modified  $C_3N_4$  configuration in the practical application, the Van Hove equation was applied to estimate the average desorption temperature  $T_d$ , as follows [36]:

$$T_d = \left( \frac{\overline{E_{b-H_2}}}{k_B} \right) \left( \frac{\Delta S}{R} - \ln P \right)^{-1} \quad (5)$$

where  $R$  denotes the gas constant,  $k_B$  represents the Boltzmann constant,  $P$  is the atmospheric pressure,  $\overline{E_{b-H_2}}$  signifies the mean adsorption energy for nine  $H_2$  atoms, which is approximately  $-0.20$  eV/ $H_2$ , and the change in entropy, represented by  $\Delta S$ , which occurs during the transition of  $H_2$  from a gas to a liquid.

#### 4. Conclusions

DFT simulations were performed to explore the possibility of storing hydrogen in pure  $C_3N_4$  nanotubes. The results show that pure  $C_3N_4$  nanotubes do not satisfy the requirements for storing  $H_2$ ; however, the addition of Sc to the nanotube allows for successful storage. According to the computed bonding energies and DOS, Sc atoms are stabilized in the macrocycle of  $C_3N_4$ , and covalent bonds are formed due to the fact that 1.83 electrons move to the N-2p states from the Sc-3d states. AIMD simulations and diffusion barriers confirm the structural stability of Sc-modified  $C_3N_4$  nanotubes at high desorption temperatures. The diffusion barrier of Sc atoms from one macrocycle to its neighbor is 5.10 eV, which avoids the creation of metal clusters. From the perspective of hydrogen storage, up to nine hydrogen molecules can be absorbed on the Sc-modified  $C_3N_4$  nanotube, with a hydrogen uptake of 7.29 wt%, which is above DOE-US requirements. The enhancement of the hydrogen storage capacity of Sc-modified  $C_3N_4$  nanotubes is due to the charge donation and back donation from the Sc-3d to H-1s. Weak van der Waals and Kubas interactions are primarily responsible for this phenomenon. Additionally, the  $H_2$  diffusion route was investigated. According to the findings,  $H_2$  diffuses in  $C_3N_4$  nanotubes more easily along the channel than along the macrocycle. Low-diffusion-barrier Sc-modified  $C_3N_4$  nanotubes create favorable conditions for adsorption. The calculated average adsorption energy and desorption temperature are  $-0.20$  eV and 258 K. For fuel cell applications, the Sc-modified  $C_3N_4$  tube is suitable as it has appropriate average adsorption energy and desorption temperatures. We assert that Sc-modified  $C_3N_4$  nanotubes are a promising and practically viable solution for high hydrogen storage.

**Supplementary Materials:** The following supporting information can be downloaded at: <https://www.mdpi.com/article/10.3390/molecules29091966/s1>, Figure S1. Geometric structures of pure  $C_3N_4$  nanotube and possible adsorption sites; Figure S2. The adsorption energy for one  $H_2$  molecule on different adsorption sites of pure  $C_3N_4$  nanotube; Table S1. The bonding energy for Sc single atom on different deposition sites of pure  $C_3N_4$  nanotube; Figure S3. Relative value of total energy variations as well as their corresponding fittings for the pristine (a) and Sc modified (b)  $C_3N_4$  nanotubes with respect to strain  $\epsilon$  along the tube axis; Figure S4. (a)–(f) The lowest-energy configuration of Sc modified  $C_3N_4$  nanotube with the successive adsorption of 1 to 8  $H_2$  molecules; Figure S5. The optimal structure of fully Sc modified  $C_3N_4$  nanotube; Table S2. The effect of defects on the bonding energy and adsorption energy; Figure S6. The optimized configuration of Sc-modified  $C_3N_4$  nanotubes adsorbing three  $H_2O$  molecules; Figure S7. PDOS for H-1s orbital versus the Sc-3d orbital in  $C_3N_4+Sc+H_2$  systems. Fermi level is set at 0 eV; Figure S8. The application diagram of Sc-modified  $C_3N_4$  nanotubes as a hydrogen storage material for storing, transporting, and releasing hydrogen [62–66].

**Author Contributions:** Supervision, L.J.; Conceptualization, L.J.; Formal analysis, S.L. and L.J.; Investigation, X.T. and L.S.; Visualization, M.W.; Writing—original draft, L.S. and M.W.; Writing—review and editing, S.L. and Z.T.; Software, C.H., T.W. and S.Y.; Funding acquisition, L.J. All authors have read and agreed to the published version of the manuscript.

**Funding:** This work is supported by the Natural Science Foundation of Henan Province (Grant No. 232300420128), the Program for Science & Technology Innovation Talents in Universities of Henan Province (Grant No. 24HASTIT013), the Young Scientist Project of Henan Province (Grant No. 225200810103), the Henan College Key Research Project (Grant Nos. 24A430002, 22A140002), the Scientific and Technological Project of Anyang City (Grant No. 2023C01GX009), the College Students Innovation Fund of Anyang Normal University (Grant No. 202310479020), and the Scientific Research Innovation Team Project of Anyang Normal University (Grant No. 2023AYSYKYCXTD04).

**Institutional Review Board Statement:** Not applicable.

**Informed Consent Statement:** Not applicable.

**Data Availability Statement:** Data are contained within the article and Supplementary Materials.

**Conflicts of Interest:** Shenbo Yang is employed by Hongzhiwei Technology (Shanghai) Co., Ltd. The remaining authors declare that the research was conducted in the absence of any commercial or financial relationships that could be construed as potential conflicts of interest.

## References

1. Zou, C.; Zhao, Q.; Zhang, G.; Xiong, B. Energy revolution: From a fossil energy era to a new energy era. *Nat. Gas Ind. B* **2016**, *3*, 1–11. [CrossRef]
2. Ouyang, L.; Huang, J.; Fang, C.; Zhang, Q.; Sun, D.; Zhu, M. The controllable hydrolysis rate for LaMg<sub>12</sub> hydride. *Int. J. Hydrogen Energy* **2012**, *37*, 12358–12364. [CrossRef]
3. Dawood, F.; Anda, M.; Shafiullah, G.M. Hydrogen production for energy: An overview. *Int. J. Hydrogen Energy* **2020**, *45*, 3847–3869. [CrossRef]
4. Yuan, Z.; Zhu, X.; Gao, X.; An, C.; Wang, Z.; Zuo, C.; Dionysiou, D.D.; He, H.; Jiang, Z. Enhancing photocatalytic CO<sub>2</sub> reduction with TiO<sub>2</sub>-based materials: Strategies, mechanisms, challenges, and perspectives. *Environ. Sci. Ecotechnol.* **2024**, *20*, 100368. [CrossRef] [PubMed]
5. Gao, X.; Cao, L.; Chang, Y.; Yuan, Z.; Zhang, S.; Liu, S.; Zhang, M.; Fan, H.; Jiang, Z. Improving the CO<sub>2</sub> Hydrogenation Activity of Photocatalysts via the Synergy between Surface Frustrated Lewis Pairs and the CuPt Alloy. *ACS Sustain. Chem. Eng.* **2023**, *11*, 5597–5607. [CrossRef]
6. Zhu, X.; Zong, H.; Pérez, C.J.V.; Miao, H.; Sun, W.; Yuan, Z.; Wang, S.; Zeng, G.; Xu, H.; Jiang, Z. Supercharged CO<sub>2</sub> photothermal catalytic methanation: High conversion, rate, and selectivity. *Angew. Chem.* **2023**, *135*, e202218694. [CrossRef]
7. Kothari, R.; Buddhi, D.; Sawhney, R.L. Comparison of environmental and economic aspects of various hydrogen production methods. *Renew. Sustain. Energy Rev.* **2008**, *12*, 553–563. [CrossRef]
8. Sinigaglia, T.; Lewiski, F.; Santos Martins, M.E.; Mairesse Siluk, J.C. Production, storage, fuel stations of hydrogen and its utilization in automotive applications—a review. *Int. J. Hydrogen Energy* **2017**, *42*, 24597–24611. [CrossRef]
9. George, L.; Saxena, S.K. Structural stability of metal hydrides, alanates and borohydrides of alkali and alkali-earth elements: A review. *Int. J. Hydrogen Energy* **2010**, *35*, 5454–5470. [CrossRef]
10. Jiang, Z.; Yuan, Z.; Duchesne, P.N.; Sun, W.; Lyu, X.; Miao, W.; Viasus Pérez, C.J.; Xu, Y.; Yang, D.; Huang, B.; et al. A living photocatalyst derived from CaCu<sub>3</sub>Ti<sub>4</sub>O<sub>12</sub> for CO<sub>2</sub> hydrogenation to methanol at atmospheric pressure. *Chem. Catal.* **2023**, *3*, 100507. [CrossRef]
11. Tai, X.; Yan, X.; Wang, L. Synthesis, Structural Characterization, Hirschfeld Surface Analysis, Density Functional Theory, and Photocatalytic CO<sub>2</sub> Reduction Activity of a New Ca(II) Complex with a Bis-Schiff Base Ligand. *Molecules* **2024**, *29*, 1047. [CrossRef]
12. Wang, L.H.; Tai, X.S. Synthesis, Structural Characterization, Hirschfeld Surface Analysis and Photocatalytic CO<sub>2</sub> Reduction Activity of a New Dinuclear Gd(III) Complex with 6-Phenylpyridine-2-Carboxylic Acid and 1,10-Phenanthroline Ligands. *Molecules* **2023**, *28*, 7595. [CrossRef]
13. Yu, X.; Wu, Z.; Xia, B.; Xu, N. Enhancement of hydrogen storage capacity of Ti–V–Cr–Mn BCC phase alloys. *J. Alloys Compd.* **2004**, *372*, 272–277. [CrossRef]
14. Wong-Foy, A.G.; Matzger, A.J.; Yaghi, O.M. Exceptional H<sub>2</sub> Saturation Uptake in Microporous Metal–Organic Frameworks. *J. Am. Chem. Soc.* **2006**, *128*, 3494–3495. [CrossRef]
15. Kudlek, E.; Dudziak, M.; Bohdziewicz, J. Influence of inorganic ions and organic substances on the degradation of pharmaceutical compound in water matrix. *Water* **2016**, *8*, 532. [CrossRef]
16. Züttel, A.; Remhof, A.; Borgschulte, A.; Friedrichs, O. Hydrogen: The future energy carrier. *Philos. Trans. R. Soc. A* **2010**, *368*, 3329–3342. [CrossRef]
17. Bhatia, S.K.; Myers, A.L. Optimum conditions for adsorptive storage. *Langmuir* **2006**, *22*, 1688–1700. [CrossRef]
18. Zhou, J.; Wang, Q.; Sun, Q.; Jena, P.; Chen, X. Electric field enhanced hydrogen storage on polarizable materials substrates. *Proc. Natl. Acad. Sci. USA* **2010**, *107*, 2801–2806. [CrossRef]
19. Ju, L.; Liu, J.; Wang, M.; Yang, S.; Liu, S. Modulation of charge in C<sub>9</sub>N<sub>4</sub> monolayer for a high-capacity hydrogen storage as a switchable strategy. *Front. Phys.* **2024**, *19*, 43208. [CrossRef]
20. Isidro-Ortega, F.J.; Pacheco-Sánchez, J.H.; Desales-Guzmán, L.A. Hydrogen storage on lithium decorated zeolite templated carbon, DFT study. *Int. J. Hydrogen Energy* **2017**, *42*, 30704–30717. [CrossRef]
21. Energy (US-DOE) Standard. Available online: <https://www.standards.doe.gov/> (accessed on 2 June 2023).
22. Gao, F.; Sun, J.T.; Meng, S. “H<sub>2</sub> sponge”: Pressure as a means for reversible high-capacity hydrogen storage in nanoporous Ca-intercalated covalent organic frameworks. *Nanoscale* **2015**, *7*, 6319–6324. [CrossRef]
23. Bellosta von Colbe, J.; Ares, J.-R.; Barale, J.; Baricco, M.; Buckley, C.; Capurso, G.; Gallandat, N.; Grant, D.M.; Guzik, M.N.; Jacob, I.; et al. Application of hydrides in hydrogen storage and compression: Achievements, outlook and perspectives. *Int. J. Hydrogen Energy* **2019**, *44*, 7780–7808. [CrossRef]
24. Heung, L.K. *Using Metal Hydride to Store Hydrogen*; Department of Energy: Washington, DC, USA, 2003.

25. Sakintuna, B.; Lamari-Darkrim, F.; Hirscher, M. Metal hydride materials for solid hydrogen storage: A review. *Int. J. Hydrogen Energy* **2007**, *32*, 1121–1140. [CrossRef]
26. Zaluski, L.; Zaluska, A.; Tessier, P.; Ström-Olsen, J.; Schulz, R. Effects of relaxation on hydrogen absorption in Fe-Ti produced by ball-milling. *J. Alloys Compd.* **1995**, *227*, 53–57. [CrossRef]
27. Floriano, R.; Leiva, D.R.; Dessi, J.G.; Asselli, A.A.C.; Jorge Junior, A.M.; Botta, W.J. Mg-based nanocomposites for hydrogen storage containing Ti-Cr-V alloys as additives. *Mater. Res.* **2016**, *19*, 80–85. [CrossRef]
28. Singh, A.K.; Singh, A.K.; Srivastava, O. On the synthesis of the Mg<sub>2</sub>Ni alloy by mechanical alloying. *J. Alloys Compd.* **1995**, *227*, 63–68. [CrossRef]
29. Li, H.; Eddaoudi, M.; O’Keeffe, M.; Yaghi, O.M. Design and synthesis of an exceptionally stable and highly porous metal-organic framework. *Nature* **1999**, *402*, 276–279. [CrossRef]
30. Kleperis, J.; Lesnicenoks, P.; Grinberga, L.; Chikvaidze, G.; Klavins, J. Zeolite as material for hydrogen storage in transport applications/CEOLĪTA KĀ ŪDENRAŽA UZGLABĀŠANAS VIDES IZPĒTE. *Latv. J. Phys. Tech. Sci.* **2013**, *50*, 59–64. [CrossRef]
31. Xia, Y.; Yang, Z.; Zhu, Y. Porous carbon-based materials for hydrogen storage: Advancement and challenges. *J. Mater. Chem. A* **2013**, *1*, 9365–9381. [CrossRef]
32. Sakintuna, B.; Yürüm, Y. Templated porous carbons: A review article. *Ind. Eng. Chem. Res.* **2005**, *44*, 2893–2902. [CrossRef]
33. Chen, Z.; Kirlikovali, K.O.; Idrees, K.B.; Wasson, M.C.; Farha, O.K. Porous materials for hydrogen storage. *Chem* **2022**, *8*, 693–716. [CrossRef]
34. Roongcharoen, T.; Impeng, S.; Chitpakdee, C.; Rungrotmongkol, T.; Jitwatanasirikul, T.; Jungsuttiwong, S.; Namuangruk, S. Intrinsic property and catalytic performance of single and double metal atoms incorporated g-C<sub>3</sub>N<sub>4</sub> for O<sub>2</sub> activation: A DFT insight. *Appl. Surf. Sci.* **2021**, *541*, 148671. [CrossRef]
35. Vaidyanathan, A.; Wagh, V.; Rout, C.S.; Chakraborty, B. High capacity reversible hydrogen storage in zirconium doped 2D-covalent triazine frameworks: Density Functional Theory investigations. *Int. J. Hydrogen Energy* **2021**, *46*, 14520–14531. [CrossRef]
36. Mahamiya, V.; Shukla, A.; Chakraborty, B. Scandium decorated C<sub>24</sub> fullerene as high capacity reversible hydrogen storage material: Insights from density functional theory simulations. *Appl. Surf. Sci.* **2022**, *573*, 151389. [CrossRef]
37. Chen, P.; Wu, X.; Lin, J.; Tan, K.L. High H<sub>2</sub> Uptake by Alkali-Doped Carbon Nanotubes Under Ambient Pressure and Moderate Temperatures. *Science* **1999**, *285*, 91–93. [CrossRef]
38. Wu, M.; Wang, Q.; Sun, Q.; Jena, P. Functionalized graphitic carbon nitride for efficient energy storage. *J. Phys. Chem. C* **2013**, *117*, 6055–6059. [CrossRef]
39. Sun, Z.; Lu, X.; Nyahuma, F.M.; Yan, N.; Xiao, J.; Su, S.; Zhang, L. Enhancing hydrogen storage properties of MgH<sub>2</sub> by transition metals and carbon materials: A brief review. *Front. Chem.* **2020**, *8*, 552. [CrossRef]
40. Tian, Z.; Liu, Y.; Wu, W.; Jiang, L.; Dong, S. Hydrogen storage of capped single-walled carbon nanotube via transition-metal doping. *Europhys. Lett.* **2013**, *104*, 36002. [CrossRef]
41. Alex, K.V.; Prabhakaran, A.; Jayakrishnan, A.; Kamakshi, K.; Silva, J.P.B.; Sekhar, K. Charge coupling enhanced photocatalytic activity of BaTiO<sub>3</sub>/MoO<sub>3</sub> heterostructures. *ACS Appl. Mater. Interfaces* **2019**, *11*, 40114–40124. [CrossRef]
42. Panigrahi, P.; Kumar, A.; Karton, A.; Ahuja, R.; Hussain, T. Remarkable improvement in hydrogen storage capacities of two-dimensional carbon nitride (g-C<sub>3</sub>N<sub>4</sub>) nanosheets under selected transition metal doping. *Int. J. Hydrogen Energy* **2020**, *45*, 3035–3045. [CrossRef]
43. Stoyanov, S.R.; Titov, A.V.; Král, P. Transition metal and nitrogen doped carbon nanostructures. *Coord. Chem. Rev.* **2009**, *253*, 2852–2871. [CrossRef]
44. Durgun, E.; Ciraci, S.; Yildirim, T. Functionalization of carbon-based nanostructures with light transition-metal atoms for hydrogen storage. *Phys. Rev. B* **2008**, *77*, 085405. [CrossRef]
45. Nachimuthu, S.; Lai, P.-J.; Jiang, J.-C. Efficient hydrogen storage in boron doped graphene decorated by transition metals—A first-principles study. *Carbon* **2014**, *73*, 132–140. [CrossRef]
46. Sun, Q.; Wang, Q.; Jena, P.; Kawazoe, Y. Clustering of Ti on a C<sub>60</sub> surface and its effect on hydrogen storage. *J. Am. Chem. Soc.* **2005**, *127*, 14582–14583. [CrossRef]
47. Nisha, V.; Moolayadukkam, S.; Paravannoor, A.; Panoth, D.; Chang, Y.-H.; Palantavida, S.; Hinder, S.J.; Pillai, S.C.; Vijayan, B.K. Cu doped graphitic C<sub>3</sub>N<sub>4</sub> for p-nitrophenol reduction and sensing applications. *Inorg. Chem. Commun.* **2022**, *142*, 109598. [CrossRef]
48. Das, T.K.; Banerjee, S.; Vishwanadh, B.; Joshi, R.; Sudarsan, V. On the nature of interaction between Pd nanoparticles and C<sub>3</sub>N<sub>4</sub> support. *Solid State Sci.* **2018**, *83*, 70–75. [CrossRef]
49. Guan, P.; Yang, B.; Liu, J.; Yin, H.; Jiang, J.; Sui, L.; Yang, S. Synthesis of novel rare-earth cerium doped C<sub>3</sub>N<sub>4</sub> nanocomposites for boosting photocatalytic H<sub>2</sub> evolution. *Chem. Phys. Lett.* **2023**, *811*, 140222. [CrossRef]
50. Dong, S.; Lv, E.; Wang, J.; Li, C.; Ma, K.; Gao, Z.; Yang, W.; Ding, Z.; Wu, C.; Gates, I.D. Construction of transition metal-decorated boron doped twin-graphene for hydrogen storage: A theoretical prediction. *Fuel* **2021**, *304*, 121351. [CrossRef]
51. Luo, Z.; Fan, X.; Pan, R.; An, Y. A first-principles study of Sc-decorated graphene with pyridinic-N defects for hydrogen storage. *Int. J. Hydrogen Energy* **2017**, *42*, 3106–3113. [CrossRef]
52. Hongzhiwei Technology, D.S., Version V2023A, China. 2021. Available online: <https://iresearch.net.cn/cloudSoftware> (accessed on 2 June 2023).
53. Blöchl, P.E. Projector augmented-wave method. *Phys. Rev. B* **1994**, *50*, 17953–17979. [CrossRef] [PubMed]

54. Perdew, J.P.; Burke, K.; Ernzerhof, M. Generalized Gradient Approximation Made Simple. *Phys. Rev. Lett.* **1996**, *77*, 3865–3868. [[CrossRef](#)]
55. Chaudhuri, S.; Graetz, J.; Ignatov, A.; Reilly, J.J.; Muckerman, J.T. Understanding the role of Ti in reversible hydrogen storage as sodium alanate: A combined experimental and density functional theoretical approach. *J. Am. Chem. Soc.* **2006**, *128*, 11404–11415. [[CrossRef](#)]
56. Xiong, R.; Sang, G.; Zhang, G.; Yan, X.; Li, P.; Yao, Y.; Luo, D.; Chen, C.A.; Tang, T. Evolution of the active species and catalytic mechanism of Ti doped NaAlH<sub>4</sub> for hydrogen storage. *Int. J. Hydrogen Energy* **2017**, *42*, 6088–6095. [[CrossRef](#)]
57. Liu, B.; Zhang, B.; Wu, Y.; Lv, W.; Zhou, S. Theoretical prediction and experimental study on catalytic mechanism of incorporated Ni for hydrogen absorption of Mg. *Int. J. Hydrogen Energy* **2019**, *44*, 27885–27895. [[CrossRef](#)]
58. Han, Z.; Yeboah, M.L.; Jiang, R.; Li, X.; Zhou, S. Hybrid activation mechanism of thermal annealing for hydrogen storage of magnesium based on experimental evidence and theoretical validation. *Appl. Surf. Sci.* **2020**, *504*, 144491. [[CrossRef](#)]
59. Grimme, S.; Antony, J.; Ehrlich, S.; Krieg, H. A consistent and accurate ab initio parametrization of density functional dispersion correction (DFT-D) for the 94 elements H-Pu. *J. Chem. Phys.* **2010**, *132*, 154104. [[CrossRef](#)]
60. Li, D.-H.; Li, Q.-M.; Qi, S.-L.; Qin, H.-C.; Liang, X.-Q.; Li, L. Theoretical Study of Hydrogen Production from Ammonia Borane Catalyzed by Metal and Non-Metal Diatom-Doped Cobalt Phosphide. *Molecules* **2022**, *27*, 8206. [[CrossRef](#)]
61. Liu, X.; Xu, Y.; Sheng, L. Al-Decorated C<sub>2</sub>N Monolayer as a Potential Catalyst for NO Reduction with CO Molecules: A DFT Investigation. *Molecules* **2022**, *27*, 5790. [[CrossRef](#)]
62. Li, X.; Dai, Y.; Ma, Y.; Li, M.; Yu, L.; Huang, B. Landscape of DNA-like inorganic metal free double helical semiconductors and potential applications in photocatalytic water splitting. *J. Mater. Chem. A* **2017**, *5*, 8484–8492. [[CrossRef](#)]
63. Liu, Y.; Du, H.; Zhang, X.; Yang, Y.; Gao, M.; Pan, H. Superior catalytic activity derived from a two-dimensional Ti<sub>3</sub>C<sub>2</sub> precursor towards the hydrogen storage reaction of magnesium hydride. *Chem. Commun.* **2016**, *52*, 705. [[CrossRef](#)]
64. Zhang, X.; Shen, Z.; Jian, N.; Hu, J.; Du, F.; Yao, J.; Gao, M.; Liu, Y.; Pan, H. A novel complex oxide TiVO<sub>3.5</sub> as a highly active catalytic precursor for improving the hydrogen storage properties of MgH<sub>2</sub>. *Int. J. Hydrogen Energy* **2018**, *43*, 23327–23335. [[CrossRef](#)]
65. Shen, Z.; Wang, Z.; Zhang, M.; Gao, M.; Hu, J.; Du, F.; Liu, Y.; Pan, H. A novel solid-solution MXene (Ti<sub>0.5</sub>V<sub>0.5</sub>)<sub>3</sub>C<sub>2</sub> with high catalytic activity for hydrogen storage in MgH<sub>2</sub>. *Materialia* **2018**, *1*, 114–120. [[CrossRef](#)]
66. Liu, Y.; Gao, H.; Zhu, Y.; Li, S.; Zhang, J.; Li, L. Excellent catalytic activity of a two-dimensional Nb<sub>4</sub>C<sub>3</sub>T<sub>x</sub> (MXene) on hydrogen storage of MgH<sub>2</sub>. *Appl. Surf. Sci.* **2019**, *493*, 431–440. [[CrossRef](#)]

**Disclaimer/Publisher's Note:** The statements, opinions and data contained in all publications are solely those of the individual author(s) and contributor(s) and not of MDPI and/or the editor(s). MDPI and/or the editor(s) disclaim responsibility for any injury to people or property resulting from any ideas, methods, instructions or products referred to in the content.